Control of the valley polarization of monolayer WSe_2 by Dexter-like coupling

2D Materials

PAPER

Control of the valley polarization of monolayer WSe_2 by Dexter-like coupling

Jakub Jasiński[1,2], Joshua J P Thompson[3], Swaroop Palai[2], Maciej Śmiertka[1], Mateusz Dyksik[1], Takashi Taniguchi[4], Kenji Watanabe[5], Michał Baranowski[1], Duncan K Maude[2], Alessandro Surrente[1], Ermin Malic[3] and Paulina Płochocka[1,2,*]

[1] Department of Experimental Physics, Faculty of Fundamental Problems of Technology, Wroclaw University of Science and Technology, 50-370 Wroclaw, Poland
[2] Laboratoire National des Champs Magnétiques Intenses, EMFL, CNRS UPR 3228, Université Grenoble Alpes, Université Toulouse, Université Toulouse 3, INSA-T, Grenoble and Toulouse, France
[3] Department of Physics, Philipps-Universität Marburg, Renthof 7 35032 Marburg, Germany
[4] International Center for Materials Nanoarchitectonics, National Institute for Materials Science, Tsukuba, Ibaraki 305-004, Japan
[5] Research Center for Functional Materials, National Institute for Materials Science, Tsukuba, Ibaraki 305-004, Japan
* Author to whom any correspondence should be addressed.

E-mail: paulina.plochocka@lncmi.cnrs.fr

Keywords: transition metal dichalcogenides, excitons, Dexter coupling, valleytronics, valley polarization

Supplementary material for this article is available online

OPEN ACCESS

RECEIVED
29 August 2023

REVISED
7 December 2023

ACCEPTED FOR PUBLICATION
3 January 2024

PUBLISHED
17 January 2024

Abstract

Intervalley scattering mechanisms strongly affect the dynamics of excitonic complexes in transition metal dichalcogenide monolayers. Here, we investigate the excitation energy dependence of the valley polarization of excitons in a WSe_2 monolayer. We observe that the valley polarization drastically decreases when the excitation is resonant with the B_{1s} resonance. This behavior can be explained by a Dexter-like coupling in the momentum space between exciton states residing in opposite valleys but with the same spin configuration. This induces a net transfer of the exciton population from the optically driven valley towards the opposite, undriven valley. We observe the long-term fingerprints of this population transfer as a vanishing valley polarization for the neutral exciton, and a negative valley polarization for biexcitonic complexes, in qualitative agreement with theoretical predictions based on a fully microscopic many-particle approach. This, together with a decrease of the PL energy when the excitation is resonant with the B_{1s} state, points to the prominent role of the Dexter-like coupling in the exciton dynamics of atomically thin semiconductors.

The spin-valley locking, characteristic of transition metal dichalcogenide (TMD) monolayers, [1–6] endows them with a binary degree of freedom, referred to as valley pseudospin. This can be initialized and read out using circularly polarized light, which addresses separately the K^+ and K^- valleys, thus creating an imbalance in the exciton populations, known as valley polarization [1–5]. Due to the large separation of the valleys in momentum space, it was thought that the polarization, once created, would prove to be very robust (long lived) in these materials. However, the polarization properties turn out to be more subtle than initially predicted. Several depolarization mechanisms have been invoked to explain the decay of the valley polarization. They can be classified based on whether they involve free carriers or excitonic complexes. In the former case, the intervalley scattering entails a spin-flip and has to be mediated by interactions with localized impurities, short-wavelength phonons or by the spin precession due to spin–orbit coupling following these scattering events [7–13]. In the latter case, the electron–hole exchange-mediated intervalley scattering acting on excitons with non-zero center of mass momentum [14] is considered to be the main source of valley depolarization [2, 15–24]. The presence of a low-lying dark exciton state, acting as an exciton reservoir, has been identified as key mechanism [25, 26] for the partial preservation of the valley polarization [15, 16, 20, 27], even for excitation far from the A exciton resonance.

Additionally, a Dexter-like mechanism, which couples the same-spin states of the A and B excitons (separated due to the large spin–orbit coupling in the

valence band of TMDs [6]) between the valleys (i.e. $A^+ \leftrightarrow B^-$ and $B^+ \leftrightarrow A^-$), as schematically presented in figure 1(a), has been investigated by both theoretical calculations and pump-probe measurements on WS_2 monolayers [28]. This mechanism has been shown to facilitate an efficient intervalley transfer of coherent excitons and has been used to explain the observed PL upconversion [29]. This intervalley transfer results in an inversion of the optically excited valley polarization on a subpicosecond timescale.

Here, we further explore the intricacies of the valley polarization mechanisms via circular-polarization resolved optical spectroscopy of monolayer WSe_2 combined with microscopic calculations. By investigating the excitation energy dependence of the valley polarization of different excitonic complexes, we reveal the prominent role played by Dexter-like coupling in determining the exciton valley polarization. We show that this mechanism enables us to control the valley polarization of different excitonic complexes using resonant optical excitation of the B exciton states. For the neutral exciton, the Dexter-like coupling results in a vanishingly small valley polarization of the neutral exciton, while for other excitonic complexes we achieve a negative valley polarization. Our results demonstrate that tuning the excitation energy represents an additional handle to control the valley polarization in monolayer WSe_2, even allowing a reversal of the optically induced polarization. Moreover, the observed effect of band gap renormalization, which occurs for excitation resonant with B_{1s} state, can also be explained in the framework of the Dexter-like coupling between the optically driven B exciton and the A exciton in the opposite valley.

We start our characterization of the hBN-encapsulated WSe_2 flake (micrograph of the sample displayed in supplementary figure S1) by measuring low-temperature photoluminescence (PL), PL excitation (PLE) and differential reflectivity spectra, shown in figures 1(b) and 2. Additional measurements and analysis allowed us to assign spectral resonances to different excitonic transitions (see supplementary figures S2, S3 and supplementary table 1). We investigate the valley properties of our sample by measuring the PL spectrum resolved in the circular polarization basis. As we show in the top panel of figure 1(b), the PL spectrum is strongly co-polarized with respect to the laser when the excitation is performed in resonance with the A_{2s} state. However, when we tune the excitation energy close to the resonance with the B_{1s}, the PL spectrum exhibits a zero or even slightly negative degree of circular polarization, as can be seen in the bottom panel of figure 1(b).

To study more systematically the influence of the pump energy on the valley polarization, we performed circular polarization resolved PLE measurements. We then calculated the degree of circular polarization, defined as $P_c = (I_{co} - I_{cr})/(I_{co} + I_{cr})$,

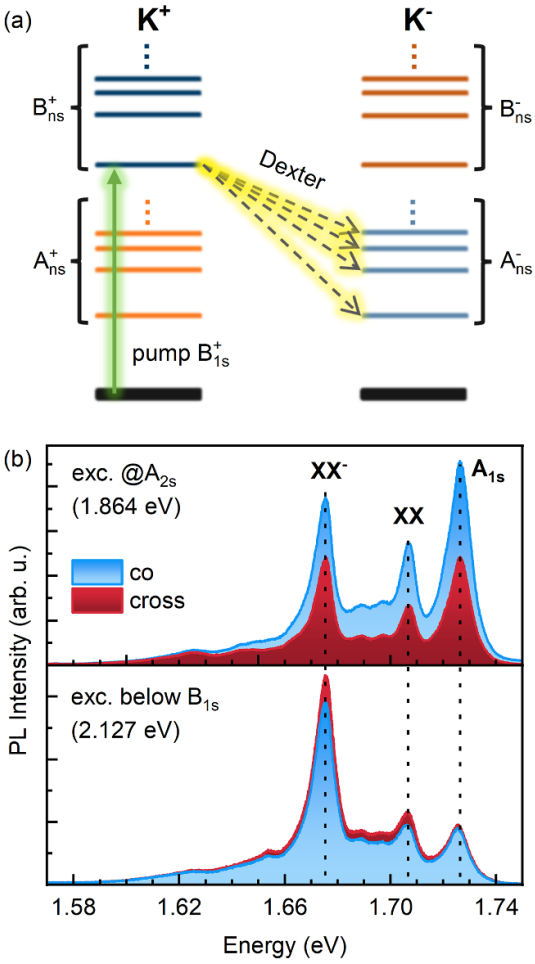

Figure 1. (a) Schematic of bright A and B exciton Rydberg states (A_{ns} and B_{ns}, respectively). Arrows denote the relevant interaction of Dexter-like intervalley coupling upon excitation of the K^+ valley resonantly with the B_{1s} state, which leads to a transfer of the bright exciton population into the opposite K^- valley. (b) PL spectra with detection of the light co-polarized (co) and cross-polarized (cross) with the circularly polarized excitation. The excitation laser was tuned in resonance with the A_{2s} transition (top panel) and at the energy corresponding to the minimum of the degree of circular polarization P_c (bottom panel) near the B_{1s} resonance. The scales in the top and bottom panels are the same for co and cross curves.

where $I_{co/cr}$ denotes the intensity of the co-polarized/cross-polarized emission, respectively. Due to spin-valley locking, this quantity enables us to directly quantify the valley polarization.

Focusing on the A_{1s} transition (see figure 2(a)), when we excite far from resonance, the P_c shows a low, positive value, which tends to increase for decreasing excitation energy. This dependence of the valley polarization on the excess energy of the excitation laser can be explained by noting that the electron–hole exchange interaction behaves effectively like an in-plane momentum-dependent magnetic field. The optically oriented valley pseudospin precesses at a frequency which depends on the value of this in-plane magnetic field, and thus depends on the excess energy of the laser [18]. This precession

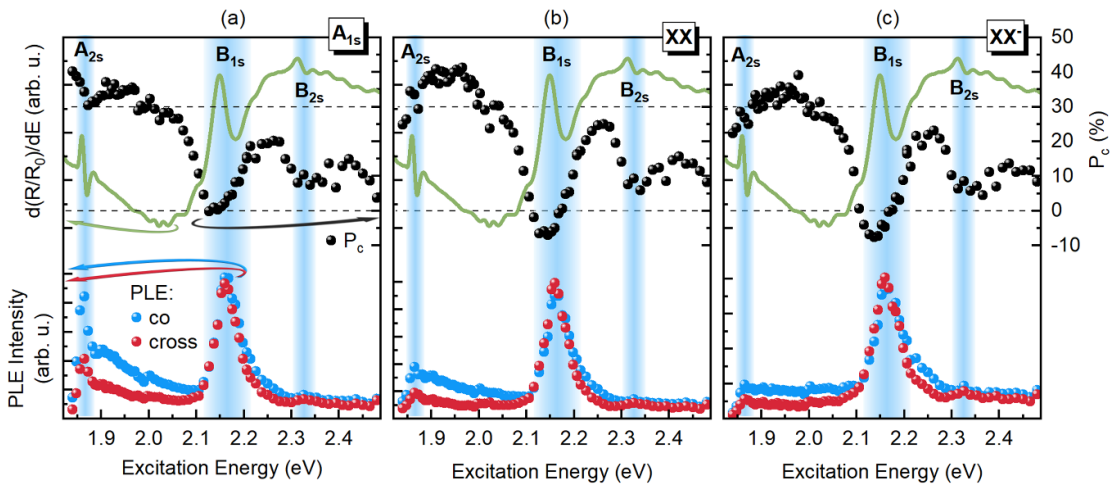

Figure 2. Excitation energy dependence of the intensity of the co- and cross-polarized emission (blue and red points, respectively) and the degree of circular polarization (P_c) (black points) for (a) A_{1s}, (b) XX and (c) XX^- excitonic transitions. Overlaid differential reflectivity spectra (green curves) allow to pinpoint the excitonic resonances. Horizontal dashed lines indicate the P_c levels of 0% and 30%.

leads to a depolarization of the exciton population. This process is less efficient for decreasing excitation energy [25]. When the pump energy is in resonance with either the B_{1s} or the B_{2s} state, the generally positive P_c decreases strongly. This decrease is especially pronounced at the B_{1s} resonance, where P_c vanishes, consistent with a strong Dexter-like coupling. Finally, when we reduce even further the excitation energy, the valley polarization exhibited by the system tends again to increase with decreasing excitation energy. This confirms that the main depolarization mechanism, which governs the intervalley dynamics far from resonance with B exciton states, is the intervalley scattering via electron–hole exchange interaction [18, 25].

By performing a similar analysis on other excitonic complexes, such as the biexciton (XX) and charged biexciton (XX^-), we notice that their polarization properties are more strongly influenced by the Dexter-induced intervalley coupling than the neutral A_{1s}, as demonstrated by the excitation energy dependence of the valley polarization plotted in figures 2(b) and (c). At an excitation resonant with the B_{1s} state, the valley polarization of the A_{1s} state reaches its lowest value of P_c of near 0%, while XX and XX^- exhibit even a negative P_c of around -7%. This suggests that the biexcitonic complexes are less prone than the neutral A_{1s} exciton to subsequent intervalley scattering processes, which lead to equalization of populations between the valleys [30]. A possible mechanism which leads to a larger negative polarization of the biexciton population relies on the Dexter-mediated transfer of the exciton population to the indirectly driven valley. There, following the relaxation processes, a population of dark excitons is established. These, together with bright excitons, form biexcitonic complexes [31, 32]. These quasiparticles undergo a slower intervalley scattering, due to the larger number of component particles [33], which allows us to observe the stronger negative valley polarization.

The drastic decrease of the valley polarization for excitation energies resonant with B exciton states can be explained by turning to the Dexter-like coupling of the same spin states in opposite valleys in the reciprocal space [28]. This Coulomb-driven interaction transfers a coherent population of excitons from the directly driven valley into the opposite valley, where they couple to photons with the opposite helicity. When the excitation is performed resonantly with the B_{ns} states, the Dexter-like coupling leads to a transfer of exciton population to the A_{ns} states of the opposite valley, which have the same spin. Therefore, these states will be preferentially populated and thus exhibit a negative valley polarization at short delays with respect to the excitation laser, as demonstrated by the results of theoretical simulation shown in figure S4 in the supplementary information. The valley polarization observed in time-integrated spectra depends then on the efficiency of different processes, such as intravalley relaxation preserving the induced valley polarization, intervalley Dexter transfer inverting the valley polarization as well as additional intervalley scattering and exchange processes, which try to equalize the valley polarization. Similar datasets consisting of excitation energy dependent degree of circular polarization of the A_{1s} exciton have already been presented [27], although the origin of the complex valley polarization dependence on the excitation energy was not discussed.

We compare now the experimental data with microscopic calculations, which model the excitation energy dependent time evolution of the valley

polarization of the A_{1s} exciton following a single excitation pulse. In the simulation, a circularly polarized laser pulse centered at 400 fs (full width at half maximum, FWHM, of 400 fs) is used to create a coherent exciton population in one of the valleys. The model tracks the time evolution of the PL from the two valleys and accounts for both intervalley Dexter-like coupling and scattering mediated via the electron–hole exchange interaction, in addition to other phonon-driven decay processes (see Methods and supplementary section for more details). We begin by showing in figure 3(a) the simulated excitation energy dependence of the valley polarization, calculated by monitoring the population of the A_{1s} state 40 fs after the onset of the laser pulse. For all excitation energies non-resonant with B_{ns} exciton states, the intensity of the PL emitted from the optically pumped valley is considerably larger than that from the valley not addressed optically. For excitation energies corresponding to resonances with B_{ns} states, conversely, the simulated valley polarization is strongly negative. This is a consequence of the efficient Dexter-like coupling between the states directly driven by the excitation laser and the A states of the opposite valley. The large negative valley polarization results from a highly efficient Dexter-like coupling due to the combination of an excitation resonant with B_{ns} states and a high coherence of the exciton population at very short delays with respect to the excitation laser [34]. In figure 3(b), we show a similar simulated excitation energy dependence of the valley polarization captured at a 4 ps delay after the onset of the excitation pulse. At this delay, the pulse is mostly over and the exciton population has lost its coherence, which greatly reduces the efficiency of the Dexter-like coupling. This, together with intervalley exchange processes, reduces the value of the negative polarization. This decrease of the negative valley polarization is reflected in the time-integrated simulated valley polarization, shown in figure 3(c), whose minimum is strongly reduced with respect to the corresponding value extracted from a coherent exciton population. Finally, we compare these results with our time-integrated experimental data, shown in figure 3(d). The strong decrease of the valley polarization when we excite resonantly with B_{1s} state can be considered a 'long-term' fingerprint of the Dexter-like coupling, whereby the initial strong negative polarization is reduced by intervalley scattering events to a near zero value.

While the excitation energy dependence of the simulated and experimental valley polarization show a good qualitative agreement, the simulated valley polarization features appear over a wider spectral range than in the experimentally determined curves. This might be related either to the discrepancy between the real and simulated parameters of the

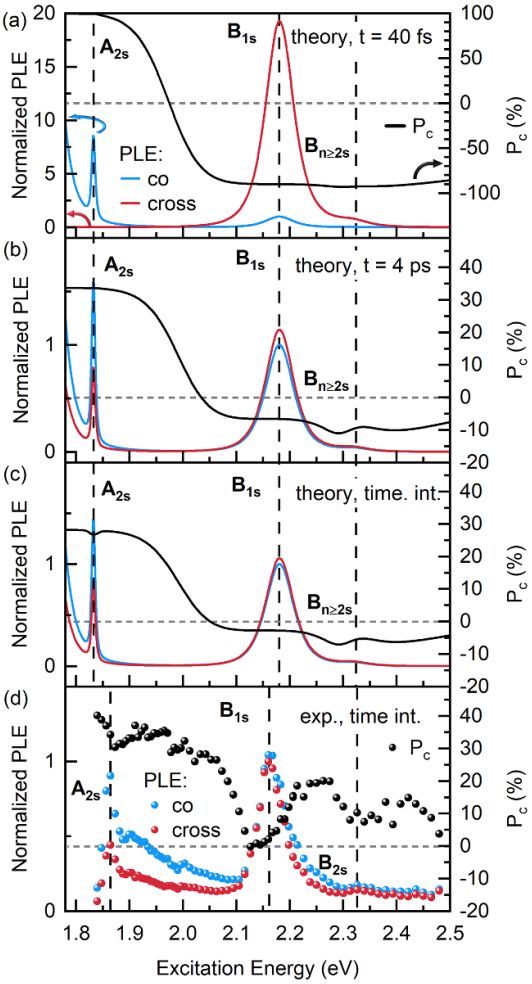

Figure 3. Calculated circular polarization resolved PLE intensity and degree of circular polarization (P_c) at time delay (a) $t = 40$ fs and (b) $t = 4$ ps after the onset of the excitation pulse, respectively. (c) PLE and P_c of the simulation time-integrated within the range of the simulation time interval (0−20 ps). (d) Experimental, time-integrated PLE intensity and P_c.

structure, which could not have been experimentally obtained e.g. the rates of the coherent/incoherent exciton transfer or other effects beyond the scope of this work.

Next, we show in figure 4(a) direct comparison of the excitation energy dependence of the valley polarization of the neutral exciton, biexciton and of the charged biexciton with the calculated valley polarization of the neutral exciton. In addition to the observation of more negative polarization preserved by the biexcitonic complexes (as compared to the neutral exciton) which we discussed above, the minimum valley polarization for all three complexes we find in our measurements is red shifted by approximately 20 meV with respect to the PLE resonance of the B_{1s} exciton, which is consistent with prior reports [27]. Both in the simulated and experimental curve the valley polarization begins to decrease at an energy considerably lower than the simulated B_{1s} resonance,

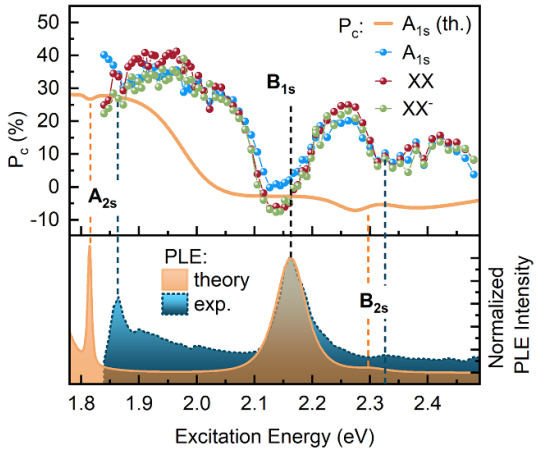

Figure 4. Comparison of simulated (for the A_{1s} exciton) and experimental (for A_{1s}, XX and XX^- excitons) P_c curves as a function of excitation energy (top) and corresponding normalized PLE intensity (bottom). The energy scale of theoretical curves is shifted by 18 meV to match the energy position of the B_{1s} exciton resonance between the experiment and simulation.

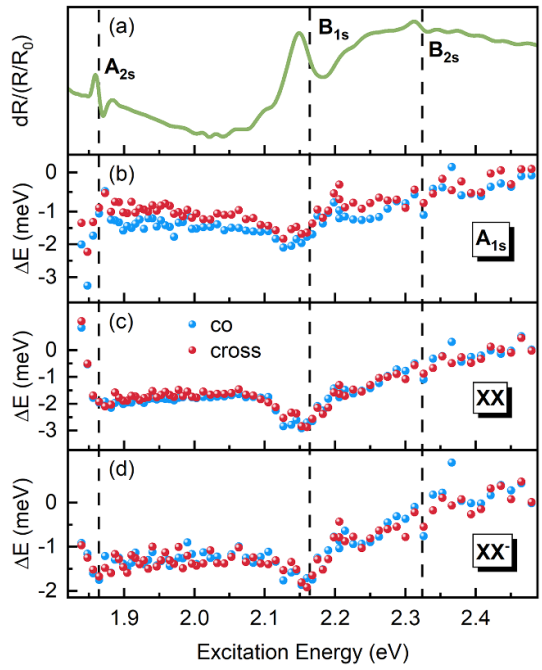

Figure 5. (a) Differential reflectivity with marked A_{2s}, B_{1s} and B_{2s} resonances (green curve). (b)–(d) Excitation energy dependence of the shift of the emission energy ΔE for the co- and cross-polarized emission (blue and red points, respectively), for (b) A_{1s}, (c) XX and (d) XX^-. Here ΔE corresponds to the shift in peak energy of a given excitonic complex with respect to its average peak energy of co and cross polarized emission at the highest excitation energy.

which is a consequence of the broadening of its resonance following its Dexter-mediated coupling to the A_{1s} state of the optically undriven valley.

The simulated valley polarization remains flat across the broadenings of the B_{ns} states. This leads to an overlap of the Dexter-like coupling effect between the B_{1s} and B_{2s} states, where the simulated valley polarization reaches its minimum value. Conversely, the experimentally determined valley polarization increases rapidly between the B_{1s} and B_{2s} states. This effect gradually counters the effect of the Dexter-like coupling, thereby increasing the valley polarization observed experimentally. The combination of the low energy onset of the negative polarization related to the broadening and the increase of the valley polarization due to the exciton population with a finite in-plane momentum leads to a ∼20 meV shift between the minimum of the valley polarization and the exciton resonance.

Finally, theory predicts that another manifestation of the Dexter induced coupling between two states in different valleys is an increase of their energy separation and a broadening of the excitonic resonances [35]. To investigate the former effect, we compare the differential reflectivity spectrum shown in figure 5(a) with the dependence on the excitation energy of the PL peak energy of the A_{1s} exciton, shown in figure 5(b), and of the neutral and charged biexciton, summarized in figures 5(c) and (d). For all the three complexes, we observe a clear red shift of the emission when the excitation laser is resonant with the B_{1s} transition. Regarding the latter effect, we have analyzed the energy dependent broadening (FWHM) of all three complexes (see supplementary figure S6). There, similarly to the aforementioned energy redshift, we observed the increase in broadening of the emission for all three complexes (approximately ∼3 meV) for excitation energy resonant with the B_{1s} transition. This effect is greater than previously reported in WS_2 [35], where the broadening of the A_{1s} state remained approximately unchanged.

In conclusion, we have demonstrated the long-term effects of the excitation-driven Dexter-like coupling mechanism on the valley polarization properties of a monolayer WSe_2. We have shown that, due to this mechanism, a valley-selective excitation resonant with the B exciton states strongly decreases the valley polarization to a near zero value for the neutral exciton (A_{1s}) or inverts the valley polarization ($\sim -7\%$) of other excitonic complexes such as XX and XX^-. This, together with the decrease of the PL peak energy of these excitonic complexes when the excitation energy is tuned in resonance with the B_{1s} exciton, is in qualitative agreement with theoretical simulations of the exciton dynamics which account for the Dexter coupling. This property could prove to be a useful tool in valleytronic devices, e.g. for optical polarization switching.

1. Methods

The sample was fabricated using flakes mechanically exfoliated on PDMS and then assembled on the silicon substrate flake by flake via dry transfer method [36]. All the experimental results have been obtained at cryogenic temperatures of ∼4 K, by cooling down the sample mounted on the cold finger of a He flow cryostat. A pulsed Ti-sapphire laser (80 MHz repetition rate, 150 fs pulse width) was used to pump an optical parametric oscillator (generated pulse width ∼300–400 fs), which was used as the excitation source in PLE measurements, in order to achieve wavelength tuning in a wide range. For excitation power dependent PL measurements, a 405 nm laser was used in either CW or pulsed mode. A 50× microscope objective with numerical aperture 0.55 was used to focus the excitation laser on the sample and collect the signal with a spatial resolution of ∼1 μm. The measurement spot of the experiments was always chosen on the flat area of the sample to avoid the impact of the strained areas such as bubbles and wrinkles that tend to form on mechanically exfoliated structures. The signal was directed to a spectrometer equipped with a liquid-nitrogen-cooled CCD camera. For reflectivity measurements, a white light source was used instead of the laser.

In order to microscopically determine the excitonic landscape in WSe_2, we use the Wannier equation [34] to derive the excitonic energy levels, ϵ^i_η, and wavefunctions, $\varphi^{\eta,i}_{\boldsymbol{k}}$, for both the A and B excitons

$$\left(\frac{\hbar^2\boldsymbol{k}^2}{2\mu^i_r}+E^i_{\mathrm{Gap}}\right)\varphi^{\eta,i}_{\boldsymbol{k}}+\sum_{\boldsymbol{k'}}V^{\boldsymbol{kk'}}_{\mathrm{Kel}}\varphi^{\eta,i}_{\boldsymbol{k'}}=\epsilon^i_\eta\varphi^{\eta,i}_{\boldsymbol{k}} \quad (1)$$

where μ_r is the reduced mass of the exciton, $\boldsymbol{k}$ is the relative momentum and E^i_{Gap} is the electronic band gap. Here, i denotes the compound index determining both the valley (K , K') and spin ($\uparrow\uparrow,\downarrow\downarrow$) of the exciton. The Coulomb interaction is described by the generalized 2D Keldysh potential, $V^{\boldsymbol{kk'}}_{\mathrm{Kel}}$, which takes into account the reduced screening in 2D systems [28]. The parameterization of this Hamiltonian and other quantities are outlined in previous studies [22, 28, 34, 35, 37].

The evolution of the valley polarization in a TMD system can be captured within the density matrix formalism. Using Heisenberg's equation of motion $i\hbar\partial_t\langle\hat{\boldsymbol{O}}\rangle=[\hat{\boldsymbol{O}},\hat{\boldsymbol{H}}]$, we derive a series of semiconductor Bloch equations [38], to track the evolution of the excitonic states. In particular, we capture the evolution of both coherent, $\hat{\boldsymbol{P}}^\eta_i$, and incoherent $\hat{\boldsymbol{N}}^\eta_{ij}$ exciton densities [37]. More details can be found in the supplementary information. Solving this series of differential equations allows us to track the time-evolution of the excitonic states and hence determine the time-resolved PLE spectra. In particular, the PLE spectra are determined by the Elliot-formula [28, 39] at fixed resonance, $\hbar\omega_{\mathrm{probe}}$, with varying excitation energy, ω, leading to the form

$$I^{\sigma\sigma',\omega_{\mathrm{probe}}}_{\mathrm{PLE}}(t,\omega)=\sum_{\xi,i,\eta}\left[|\langle\hat{\boldsymbol{P}}^{\eta\xi}_i(t,\omega,\sigma)\rangle|^2+\langle\hat{\boldsymbol{N}}^{\eta\xi}_{ij}(t,\omega,\sigma)\rangle\right]\times\Im\left(\frac{|\varphi^{\eta,i}(r=0)|^2|\boldsymbol{M}^{i\xi}\cdot\hat{\boldsymbol{e}}_{\sigma'}|^2}{\epsilon^i_\eta-\hbar\omega_{\mathrm{probe}}+i\gamma}\right)$$

where σ (σ') describes the polarization of the exciting (measured) light. The magnitude of each excitonic signature depends on the optical matrix element and the polarization vector of the emitted light $\hat{\boldsymbol{e}}_{\sigma'}$, as well as $|\varphi^{\eta,i}(\mathrm{r}=0)|$, which describes the probability of finding the electron and hole at the same position, for a given excitonic state. The broadening of the PLE is determined by γ, which we calculate microscopically [34].

Data availability statement

All data that support the findings of this study are included within the article (and any supplementary files).

Acknowledgments

The Marburg group has received funding from Deutsche Forschungsgemeinschaft via CRC 1083. This study has been partially supported through the EUR Grant NanoX n° ANR-17-EURE-0009 in the framework of the'Programme des Investissements d'Avenir'. K W and T T acknowledge support from JSPS KAKENH I (Grant Numbers 19H05790, 20H00354 and 21H05233). M B acknowledges funding from the National Science Centre Poland within the SONATA BIS program (Grant No. 2020/38/E/ST3/00194) and OPUS LAP (2021/43/I/ST3/01357). J J acknowledges funding from the National Science Centre Poland within the Preludium Bis 1 (2019/35/O/ST3/02162) program.

ORCID iDs

Jakub Jasiński https://orcid.org/0000-0003-0631-9461
Kenji Watanabe https://orcid.org/0000-0003-3701-8119
Michał Baranowski https://orcid.org/0000-0002-5974-0850
Alessandro Surrente https://orcid.org/0000-0003-4078-4965
Paulina Płochocka https://orcid.org/0000-0002-4019-6138

References

[1] Yao W, Xiao D and Niu Q 2008 *Phys. Rev.* B **77** 235406
[2] Xiao D, Liu G-B, Feng W, Xu X and Yao W 2012 *Phys. Rev. Lett.* **108** 196802

[3] Xu X, Yao W, Xiao D and Heinz T F 2014 *Nat. Phys.* **10** 343
[4] Yu H, Cui X and Yao W 2015 *Natl Sci. Rev.* **2** 57
[5] Stier A V, McCreary K M, Jonker B T, Kono J and Crooker S A 2016 *Nat. Commun.* **7** 10643
[6] Zhu Z Y, Cheng Y C and Schwingenschlögl U 2011 *Phys. Rev.* B **84** 153402
[7] Schmidt H, Yudhistira I, Chu L, Neto A C, Özyilmaz B, Adam S and Eda G 2016 *Phys. Rev. Lett.* **116** 046803
[8] Wang L and Wu M 2014 *Phys. Rev.* B **89** 115302
[9] Song Y and Dery H 2013 *Phys. Rev. Lett.* **111** 026601
[10] Ochoa H and Roldán R 2013 *Phys. Rev.* B **87** 245421
[11] Lu H-Z, Yao W, Xiao D and Shen S-Q 2013 *Phys. Rev. Lett.* **110** 016806
[12] Dey P, Yang L, Robert C, Wang G, Urbaszek B, Marie X and Crooker S A 2017 *Phys. Rev. Lett.* **119** 137401
[13] Kim J *et al* 2017 *Sci. Adv.* **3** e1700518
[14] Maialle M, Silva E d A and Sham L 1993 *Phys. Rev.* B **47** 15776
[15] Zeng H, Dai J, Yao W, Xiao D and Cui X 2012 *Nat. Nanotechnol.* **7** 490
[16] Zhu C, Zhang K, Glazov M, Urbaszek B, Amand T, Ji Z, Liu B and Marie X 2014 *Phys. Rev.* B **90** 161302
[17] Yu H, Liu G-B, Gong P, Xu X and Yao W 2014 *Nat. Commun.* **5** 3876
[18] Yu T and Wu M 2014 *Phys. Rev.* B **89** 205303
[19] Wang Y-T, Luo C-W, Yabushita A, Wu K-H, Kobayashi T, Chen C-H and Li L-J 2015 *Sci. Rep.* **5** 8289
[20] Plechinger G, Nagler P, Arora A, Schmidt R, Chernikov A, Del Águila A G, Christianen P C, Bratschitsch R, Schüller C and Korn T 2016 *Nat. Commun.* **7** 12715
[21] Dery H 2016 *Phys. Rev.* B **94** 075421
[22] Schmidt R, Berghauser G, Schneider R, Selig M, Tonndorf P, Malic E, Knorr A, Michaelis de Vasconcellos S and Bratschitsch R 2016 *Nano Lett.* **16** 2945
[23] Hao K *et al* 2017 *Nat. Commun.* **8** 15552
[24] Yan T, Qiao X, Tan P and Zhang X 2015 *Sci. Rep.* **5** 15625
[25] Baranowski M, Surrente A, Maude D K, Ballottin M, Mitioglu A, Christianen P, Kung Y, Dumcenco D, Kis A and Plochocka P 2017 *2D Mater.* **4** 025016
[26] Tornatzky H, Kaulitz A-M and Maultzsch J 2018 *Phys. Rev. Lett.* **121** 167401
[27] Wang G *et al* 2015b *Nat. Commun.* **6** 10110
[28] Berghäuser G, Bernal-Villamil I, Schmidt R, Schneider R, Niehues I, Erhart P, Michaelis de Vasconcellos S, Bratschitsch R, Knorr A and Malic E 2018 *Nat. Commun.* **9** 971
[29] Manca M *et al* 2017 *Nat. Commun.* **8** 14927
[30] Li Z *et al* 2018 *Nat. Commun.* **9** 3719
[31] Nagler P *et al* 2018 *Phys. Rev. Lett.* **121** 057402
[32] Cunningham P D, Hanbicki A T, Reinecke T L, McCreary K M and Jonker B T 2019 *Nat. Commun.* **10** 5539
[33] Singh A *et al* 2016 *Phys. Rev. Lett.* **117** 257402
[34] Selig M, Berghäuser G, Raja A, Nagler P, Schüller C, Heinz T F, Korn T, Chernikov A, Malic E and Knorr A 2016 *Nat. Commun.* **7** 13279
[35] Bernal-Villamil I *et al* 2018 *2D Mater.* **5** 025011
[36] Castellanos-Gomez A, Buscema M, Molenaar R, Singh V, Janssen L, Van Der Zant H S and Steele G A 2014 *2D Mater.* **1** 011002
[37] Brem S, Selig M, Berghaeuser G and Malic E 2018 *Sci. Rep.* **8** 8238
[38] Kira M and Koch S W 2006 *Prog. Quantum Electron.* **30** 155
[39] Koch S, Kira M, Khitrova G and Gibbs H 2006 *Nat. Mater.* **5** 523